Submitted to ADVANCED MATERIALS

DOI: 10.1002/adma.201603158
Article type: Communication

Taming liquid crystal self-assembly: the multifaceted response of nematic and smectic shells to polymerization

*JungHyun Noh, Benjamin Henx and Jan P. F. Lagerwall**

JungHyun Noh, Benjamin Henx and Prof. Jan P. F. Lagerwall
University of Luxembourg, Physics & Materials Science Research Unit,
162a Avenue de la Faiencerie , L-1511, Luxembourg
E-mail: jan.lagerwall@lcsoftmatter.com

Keywords: liquid crystals, polymerization, spherical topology, topological defects, microfluidics

Liquid crystal-mediated self-assembly has emerged as a potent tool for advanced materials research and development, with particularly compelling opportunities opened by operating with topological defects. Defects enable controlled one-,[1–5] two-[6] and three-dimensional[7] colloidal assembly in liquid crystals (LCs) of nematic type (long-range orientational order but no positional order). Conversely, complex defect line arrangements, even including knots, can be induced in LCs by introduction of appropriately designed colloidal particles.[8,9] Further concepts range from nanoscopic templating in defect lines[10,11] to actuators with specific folding or pumping actions.[12–15] In flat samples, topological defects can be introduced by advanced photopatterning,[16] but defects in fact occur spontaneously in LC droplets or shells thanks to their spherical topology. If the director **n** (the average LC molecule orientation) has a component in the spherical interface, the director field **n**(**r**) must contain topological surface defects, summing up to a total topological charge of +2.[17] An everyday analogy are the poles of the Earth, which are unavoidable topological defects in the meridional field. Curvature-induced LC defects are now explored in innovative sensing approaches: when threading nematic droplets on biofibers, defect rings develop that reveal information on the fiber morphology,[18] and topological defects in nematic droplets enable detection of endotoxin with extraordinary sensitivity.[19] Another application avenue was proposed by Nelson:[20]

because a tetrahedral defect arrangement minimizes the free energy of spherically symmetric nematic shells, they could generate particles with interactions directed for diamond-like colloid crystallization, of large interest for the photonics industry. However, when the first nematic shells were realized experimentally,[21] Fernandez-Nieves et al. found that the LC reduces its free energy further by breaking spherical symmetry, collecting all defects in a localized region with minimum shell thickness. Although the tetrahedral arrangement can be recovered by making the shell very thin,[22] this illustrates the challenge in harnessing LC-mediated self-assembly. The large parameter space is a blessing through the many possible outcomes, but a curse through the difficulty in accounting for all of them. There is thus a clear need to identify a method to tame the self-assembly in LC shells, without restricting the opportunities.

Another serious problem is the limited shell lifetime, on the order of days or less. Adjacent shells coalesce into a droplet and isolated shells collapse due to diffusion of the surrounding isotropic phases through the shell.[23] Moreover, while the temperature sensitivity of the defect arrangement in shells undergoing a phase transition from nematic (N) to smectic-A (SmA; 1D positional order in a layered molecule arrangement) conveniently allows tuning of the defect configuration[24–26]—a fact we will be taking advantage of below—it also means that uncontrolled temperature variations can trigger undesired changes in the types and arrangements of defects. In any attempt to apply LC shells a means to ensure long-term shell stability and render a desired defect configuration permanent, is required.

In this paper we show that photopolymerization of reactive mesogens (RMs)[27,28] in LC shells solves both problems. A low RM concentration (5%) is sufficient to fix a certain defect configuration and dramatically extend the shell lifetime. Moreover, when polymerizing at a temperature near either boundary of the nematic phase range, we surprisingly find that the process induces a transition into the adjacent phase.

Using capillary microfluidics we prepare planar-aligned shells based on the commonly studied compound 8CB. With 5wt% reactive mesogen RM257 and 1wt% photoinitiator (thus 20wt% with respect to RM) the phase sequence is SmA 29.1 N 42.0 Iso./°C. As discussed in the Supporting Information (SI), the reason for the comparatively high concentration of photoinitiator is that the excess initiator counteracts the polymerization-inhibiting oxygen diffusing into the system from the surrounding aqueous phases. At 35.0°C, in the middle of the N phase, four closely spaced +1/2 defects are seen at the thinnest, bottom, part of the shells (**Figure 1b**). Polymerization is initiated at this temperature by UV irradiation of the sample. Figure 1b shows that the texture on the bottom shell half is retained after polymerization, with identical defect arrangement. The top half of the shell now exhibits slight scattering from small grains; we will come back to their origin below.

We heat the polymerized shell over the clearing point T_{NI} of 8CB and then cool it back to the N phase, see **Figure 2** and Movie 1 in the SI. At 42.5°C the defect texture disappears and the shell appears mainly isotropic (Figure 2b). However, by rotating the crossed polarizers by 45° (Figure 2c) we see that the birefringence, Δn, is still high, although 8CB is isotropic at this temperature. This shows that the polymer network on the top half of the shell is dense and well aligned. It has here been templated into a uniform alignment by the LC mixture, which was in the nematic state at the temperature of polymerization, in a uniform, defect-free arrangement on the top shell half.

Importantly, the facts that the defect pattern disappears on heating and that the lower half of the shell appears to have $\Delta n \approx 0$ demonstrates that the bottom half contains only a low density polymer network, allowing it to go apparently isotropic upon heating. Due to density mismatch between LC and inner phase the shell is the thickest at the top and the thinnest at the bottom, making the reactive LC mixture at the bottom much more exposed to the polymerization-inhibiting oxygen, diffusing from the surrounding aqueous phases, than at the

top. We believe that this is the explanation to the denser polymer network in the uniform, thick part of the shell, the polymerization there being more efficient than in the strongly exposed bottom region, in which the defects are localized.

Although the defect pattern disappears on heating as the bottom of the shell turns isotropic, the original nematic texture, with the defects positioned in the exact same places as before, is recovered on cooling back to 35°C (Figure 2d). This confirms that the defects are successfully locked into place by the polymer network. This is remarkable since the network at the bottom half of the shell is so sparse that there is no trace of birefringence, nor of any defects, here after the LC turns isotropic on heating.

Using another set of shells, we again polymerize in the nematic phase but at 41.5°C, close to T_{NI} (Figure 1a). Before polymerization the texture is similar to that in Figure 1b, but this time, immediately upon UV irradiation, the shell turns black between crossed polarizers, indicating a transition to an isotropic state (Figure S3a-c in SI). Broer and co-workers reported isotropization upon photopolymerization of flat nematics near T_{NI}.[29] The heat released from the polymerization reaction elevates the temperature above T_{NI}. Without nematic order guiding the further chain growth, the polymer develops into a disordered network. Indeed, when cooling back to 35°C countless domains appear in our shell (Figure S3d and Movie 2 in SI). The random polymer network now templates an unnatural mosaic-like configuration of the N phase.

If we instead cool the pristine nematic shells towards T_{NS} prior to initiating polymerization, the four defects move up towards the equator. As explained in references,[24,25,30] this is due to the diverging free energy cost of bend deformation of **n(r)** upon approaching the SmA phase, and the fact that such deformation can be avoided in the shell only if all defects are arranged on a great circle. When we polymerize the shells via UV irradiation, the defects remain roughly in place but they are somewhat blurred and the surrounding texture is distorted, see

Figure 1c.

Carrying out the polymerization very close to T_{NS}, where the defects are even closer to the equator, a more drastic change in texture takes place, see Figure 1d-e. Unexpectedly, upon UV irradiation a spherical lune pattern develops all around the shell. Especially after polymerization at 29.15°C this pattern is highly regular. By refocusing between top and bottom we see that the lunes run parallel to the original **n**(**r**) (Figure 1e).

The defect movement and the lune patterns observed during polymerization close to T_{NS} remind us of the textural development in pure 8CB shells during cooling through the N-SmA phase transition. As discussed in references[24,25] the lune pattern signifies a buckling instability triggered by the incompatibility between smectic order and spherical shell geometry. The appearance of this texture in our experiments thus suggests that polymerization induces smectic order. We note that any heating effect from polymerization, driving the shell in Figure 1a past T_{NI}, must still be active. Thus, the smectic phase is induced by polymerization although the temperature is in fact increasing.

We propose a plausible scenario for the smectic-inducing effect, illustrated schematically in Figure S5 in the SI. The asymmetric mesogen design of 8CB leads to antiparallel association into dimers,[31] with length about 3.56 nm. This closely matches the 3.6 nm length of the RM257 mesogen. On cooling towards T_{NS}, the 8CB dimers organize with fluctuating local smectic order into so-called cybotactic clusters.[32] When we then initiate polymerization of the RM257 mesogens, aligned along **n**(**r**), chain propagation takes place perpendicular to **n**, along a plane that effectively defines a smectic layer boundary. This is because the acrylate groups reacting to form the polymer are at each end of the RM257 mesogen. Because of the geometric match between RM257 and dimerized 8CB, we believe that the chain propagation renders the cybotactic clusters permanent in time and extends their range in space to the point

of divergence, thus inducing the transition to SmA. In contrast, at high temperature there are no cybotactic clusters, and the RM fraction is too small to propagate smectic order over long distances. Polymerization then induces tiny smectic-like islands, probably the scattering grains in Figure 1b.

To find support for this conjecture and to confirm the role of cybotactic clusters, and also to rule out any odd-even effect with respect to the alkyl chain length,[31] we repeated the experiments with shells based on 5CB, 7CB and 9CB, respectively, with the same amount of RM and photoinitiator. 5CB and 7CB have no smectic phase in their phase sequences, thus they never develop cybotactic clusters, whereas 9CB has the same phase sequence as 8CB but it has an odd-numbered alkyl chain. As shown in Figure S6 and S7 in the SI, RM polymerization induced no smectic phase in 5CB- or 7CB-based shells, regardless of the polymerization temperature. In contrast, when we polymerized the RM in nematic shells based on 9CB, close to T_{NS}, we saw the defect motion and spherical lune formation (Figure S8), just as in the corresponding experiments on 8CB-based shells.

We have repeatedly investigated polymer-stabilized shells as a function of time, finding no change in shape or texture over the time scale of several months. We thus expect that the polymerization of the RM component renders the shell truly long-term stable. Moreover, we test for temperature stability by studying the texture development upon cooling of the 7CB shells polymerized in the nematic phase. The shells are cooled far below the crystallization temperature (30°C for pure 7CB, somewhat lower for the mixture). As shown in Figure S9 in the SI, the shells maintain their spherical shape without collapsing and there is no trace of crystallization. The nematic texture with locked-in defect arrangement is perfectly retained, confirming the excellent stabilization.

Finally, we also cool an 8CB+RM257 shell slowly into SmA before initiating polymerization, such that the striped lune pattern characteristic of SmA shells can develop as an equilibrium

texture,[24,25] without any influence of polymer chain growth. When this pattern is stable, polymerization is initiated by UV irradiation. This time, no further change is detected in the texture, see **Figure 3a-c** and Movie 3 in the SI. As the shell is heated up through the original nematic and then isotropic phase ranges, the striped lune texture remains. The only traces of phase transitions are reductions in birefringence and the disappearance of some of the finest chevron modulation.

To image also the shell back side we rapidly flip a capillary, filled with a suspension of shells polymerized in the SmA phase, upside down, see Figure 3d-f and Movie 4 in the SI. This provides striking further evidence of the reduced polymer network density at the shell bottom. Because of the shell asymmetry the center of mass is now above the geometric center, and we can follow how gravity slowly rotates the shell back to its initial orientation. The original shell bottom appears like an extremely thin patch that closes up the heavily striped polymerized part of the shell. In fact, the patch is so thin that it appears isotropic between crossed polarizers, the only birefringent areas being small islands which most likely are isolated patches of polymerized RM257.

We end the paper by briefly discussing application opportunities. In the context of bio-sensing we may utilize the same principles that so far were demonstrated with nematic droplets,[18,19] the shells introducing some potential advantages. Shells can be much larger, yet with excellent control of the ground state alignment, thus simplifying texture analysis. Complex director fields can be induced by combining different alignment agents, allowing e.g. bend from inside to outside, inducing specific defect configurations.[33,34] It is important that the defect-containing side of a polymer-stabilized shell can still go through structural rearrangements, like the nematic-isotropic transition, as it means that the sensing functionality should be retained. As shown in the SI, the polymerization conditions can be tuned such that the polymer network is continuous only through the top half of the shell, removing the

fixation of the defects at the bottom. For some sensing applications this may be desirable.

With optimized mixture components we could incorporate much larger fractions of RM, allowing us to take advantage of the structure formation driven by LC self-assembly in the shell to create polymer materials with enhanced network morphology. For instance, polymerization in the SmA shell locks the spherical lunes, and to some extent even the secondary modulation, into place, as seen by these patterns remaining upon heating beyond the clearing point of 8CB (Figure 3). This means that we can easily obtain a highly anisotropic polymer network, with a complex yet regular arrangement over macroscopic areas, from uniform alignment on the shell inside to a zig-zag modulation on the shell outside.[24,25] We would then have a curved polymer shell that to some extent resembles the eye's cornea, gaining exceptional mechanical strength from a radially periodic orientational modulation of its highly anisotropic collagen network.[35] With respect to Nelson's proposed new colloidal chemistry,[20] polymerization of the shells represents a major step forward. Our work shows that nematic shells can be made durable by polymerization, with the defects and their arrangement intact.

In conclusion, with polymer stabilization of LC shells we can turn short-lived fluid objects of academic interest into long-term stable systems that are robust enough to be realistically considered for applications. If the RMs in a planar-aligned nematic shell are polymerized at a temperature far away from phase transitions, the director field throughout the shell is preserved, with topological defects locked into the configuration adapted prior to polymerization. Our work provides a new illustration of the power of spherical topology applied to LC self-assembly. Since numerous options exist to further modify the structure within the shell prior to polymerization, e.g. by using chiral LCs or by combining different aligning agents, polymerization of LC shells opens a vast and prolific playground for advanced materials design.

Experimental Section

Full details are provided in the SI. Shells were produced using a coaxial glass capillary microfluidic set-up,[36] a mixture of water and glycerol (50/50 volume ratio) with 1 wt.-% of polyvinyl alcohol (PVA, Mw 13,000 - 23,000 g mol ^{1}, 87-88% hydrolyzed) used for inner and outer phases. Density mismatch lowers the inner drop to the bottom of the shell, which is thus the thinnest point. Shell suspensions are filled into flat rectangular glass capillaries for polarizing optical microscopy (Olympus BX-51), the temperature controlled by a hot stage (Linkam T95-PE).

To avoid premature polymerization, a yellow-green filter was inserted in the microscope. Photopolymerization was initiated using a UVATA LED UV curing system (8800 mW/cm^2 at full power, 365 nm). Illumination was at 45° to the sample plane and about 3 cm above the sample. For polymerization, the sample was exposed at maximum power for 1 minute.

Supporting Information

Supporting Information is available online from the Wiley Online Library or from the author.

Acknowledgements

We thank Merck Korea for the sample of RM257. Financial support from the Fonds National de la Recherche Luxembourg, PhD Grant 6992111, and the European Research Council (ERC, consolidator project INTERACT, grant code 648763), is gratefully acknowledged.

Received: ((will be filled in by the editorial staff))
Revised: ((will be filled in by the editorial staff))
Published online: ((will be filled in by the editorial staff))

[1] H. Agha, Y. Galerne, *Phys. Rev. E*, **2016**, *93*, 4.

[2] Y. Galerne, *Phys. Rev. E*, **2016**, *93*, 042702.

[3] E. Lee, Y. Xia, J. Ferrier, Robert C., H.-N. Kim, M. A. Gharbi, K. J. Stebe, R. D. Kamien, R. J. Composto, S. Yang, *Adv. Mater.*, **2016**, *28*, 2731.

[4] H. Agha, J.-B. Fleury, Y. Galerne, *Eur. Phys. J. E*, **2012**, *35*, 82.

[5] J.-B. Fleury, D. Pires, Y. Galerne, *Phys. Rev. Lett.*, **2009**, *103*, 267801.

[6] I. Musevic, M. Skarabot, U. Tkalec, M. Ravnik, S. Zumer, *Science*, **2006**, *313*, 954.

[7] A. Nych, U. Ognysta, M. Skarabot, M. Ravnik, S. Zumer, I. Musevic, *Nat. Commun.*, **2013**, *4*, 1489.

[8] U. Tkalec, M. Ravnik, S. Copar, S. Zumer, I. Musevic, *Science*, **2011**, *333*, 62.

[9] A. Martinez, M. Ravnik, B. Lucero, R. Visvanathan, S. Zumer, I. Smalyukh, *Nat. Mater.,* **2014**, *13*, 258.

[10] X. Wang, Y. Kim, E. Bukusoglu, B. Zhang, D. Miller, N. Abbott, *Phys. Rev. Lett.*, **2016**, *116*, 147801.

[11] X. Wang, D. Miller, E. Bukusoglu, J. de Pablo, N. Abbott, *Nat. Mater.,* **2015**, *15*, 106.

[12] M. McConney, A. Martinez, V. Tondiglia, K. Lee, D. Langley, I. Smalyukh, T. White, *Adv. Mater.*, **2013**, *25*, 5880.

[13] R. R. Kohlmeyer, J. Chen, *Angew. Chem. Int. Ed*., **2013**, *52*, 9234.

[14] D. Liu, C. W. M. Bastiaansen, J. M. J. den Toonder, D. J. Broer, *Angew. Chem. Int. Ed.*, **2012**, *51*, 892.

[15] E.-K. Fleischmann, H.-L. Liang, N. Kapernaum, F. Giesselmann, J. P. F. Lagerwall, R. Zentel, *Nat. Commun.,* **2012**, *3*, 1178.

[16] Y. Guo, M. Jiang, C. Peng, K. Sun, O. Yaroshchuk, O. Lavrentovich, Q.-H. Wei, *Adv. Mater.*, **2016**, *28*, 2353.

[17] T. Lopez-Leon, A. Fernandez-Nieves, *Colloid. Polym. Sci.,* **2011**, *289*, 345.

[18] L. Aguirre, A. de Oliveira, D. Sec, S. Copar, P. Almeida, M. Ravnik, M. Godinho, S. Zumer, *Proc. Natl. Acad. Sci. U.S.A.*, **2016**, *113*, 1174.

[19] I.-H. Lin, D. S. Miller, P. J. Bertics, Paul, C. J. Murphy, J. J. de Pablo, N. L. Abbott, *Science*, **2011**, *332*, 1297.

[20] D. R. Nelson, *Nano. Lett.*, **2002**, *2*, 1125.

[21] A. Fernandez-Nieves, V. Vitelli, A. Utada, D. R. Link, M. Marquez, D. R. Nelson, D. A. Weitz, *Phys. Rev. Lett.*, **2007**, *99*, 157801.

[22] T. Lopez-Leon, V. Koning, K. B. S. Devaiah, V. Vitelli, A. Fernandez-Nieves, *Nat.*

Phys., **2011**, *7*, 391.

[23] J. Noh, K. Reguengo De Sousa, J. P. F. Lagerwall, *Soft Matter*, **2016**, *12*, 367.

[24] H.-L. Liang, S. Schymura, P. Rudquist, J. Lagerwall, *Phys. Rev. Lett.,* **2011**, *106*, 247801.

[25] T. Lopez-Leon, A. Fernandez-Nieves, M. Nobili, C. Blanc, *Phys. Rev. Lett.,* **2011**, *106*, 247802.

[26] D. Sec, T. Lopez-Leon, M. Nobili, C. Blanc, A. Fernandez-Nieves, M. Ravnik, S. Zumer, *Phys. Rev. E,* **2012**, *86,* 020705.

[27] I. Dierking, P. Archer, *RSC Adv.,* **2013**, *3*, 26433.

[28] D. J. Broer, J. Boven, G. N. Mol, G. Challa, *Makromol. Chem.*, **1989**, *190*, 2255.

[29] D. J. Broer, N. Grietje, N. Mol, *Makromol. Chem.,* **1991**, *192,* 59.

[30] H. Shin, M. Bowick, X. Xing, *Phys. Rev. Lett.,* **2008**, *101*, 037802.

[31] D. Demus, J. W. Goodby, G. Gray, H.-W. Spiess, V. Vill, *Handbook of liquid crystals.*, Wiley-VCH, Weinheim, **1998**.

[32] A. De Vries, *Mol. Cryst. Liq. Cryst.*, **1970**, *10*, 219 .

[33] H. Liang, J. Noh, R. Zentel, P. Rudquist, J. Lagerwall, *Philos. Transact. A Math. Phys. Eng. Sci.,* **2013**, *371*, 20120258.

[34] H.-L. Liang, R. Zentel, P. Rudquist, J. Lagerwall, *Soft Matter,* **2012**, *8*, 5443.

[35] H. Aghamohammadzadeh, R. Newton, K. Meek, *Structure*, **2004**, *12*, 249.

[36] A. Utada, L. Chu, A. Fernandez-Nieves, D. Link, C. Holtze, D. Weitz, *MRS Bull.,* **2007**, *32*, 702.

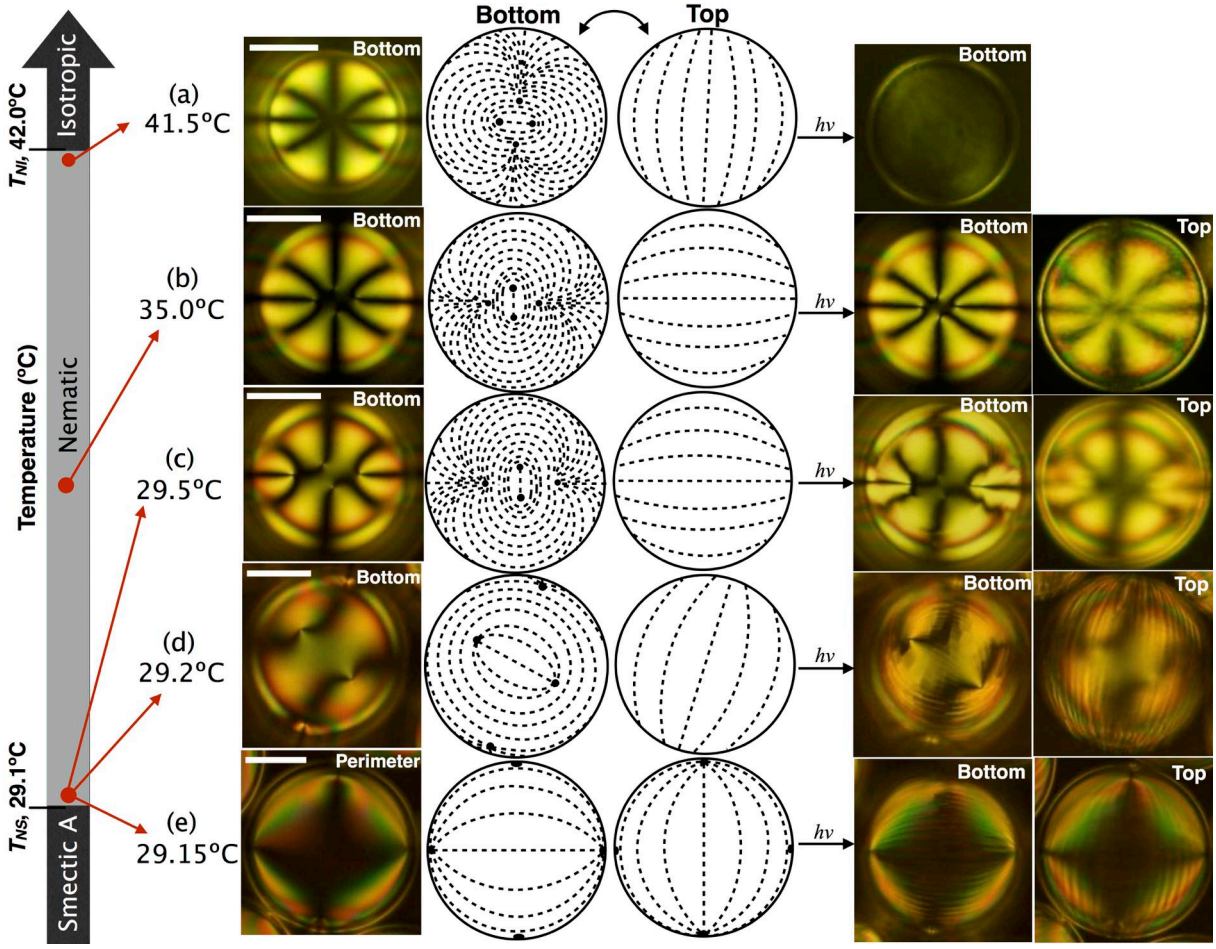

Figure 1. Polarizing microscopy textures of pristine 8CB+RM257 nematic shells (left- most images) and schematic drawings of n(r) on the bottom and top surfaces, respectively, at different nematic temperatures. The right-most images show textures after polymerization at each temperature, with focus on the bottom and top of the shell, respectively. All scale bars are 50 μm; the shell thickness is below 5 μm.

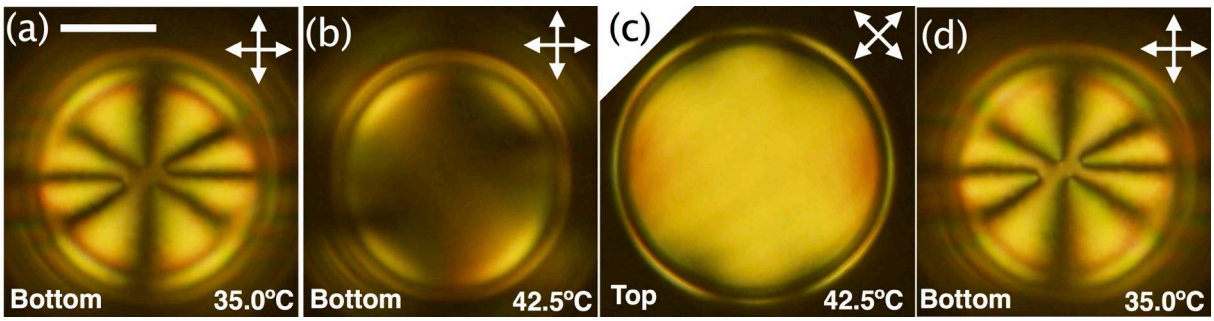

Figure 2. Texture changes on heating and cooling (10 K min^{-1}) an 8CB+RM257 shell after polymerization at 35°C in the nematic phase; (a) Nematic texture with four +1/2 defects at the bottom of the polymerized shell at 35°C, (b) texture at 42.5°C, which is above the clearing

point (42.0°C). (c) A strongly birefringent polymer network is revealed by rotating the crossed polarizers by 45°. (d) On cooling to the nematic phase at 35°C, the original defect configuration is fully recovered. The scale bar is 50 μm and the focal plane is indicated in each image.

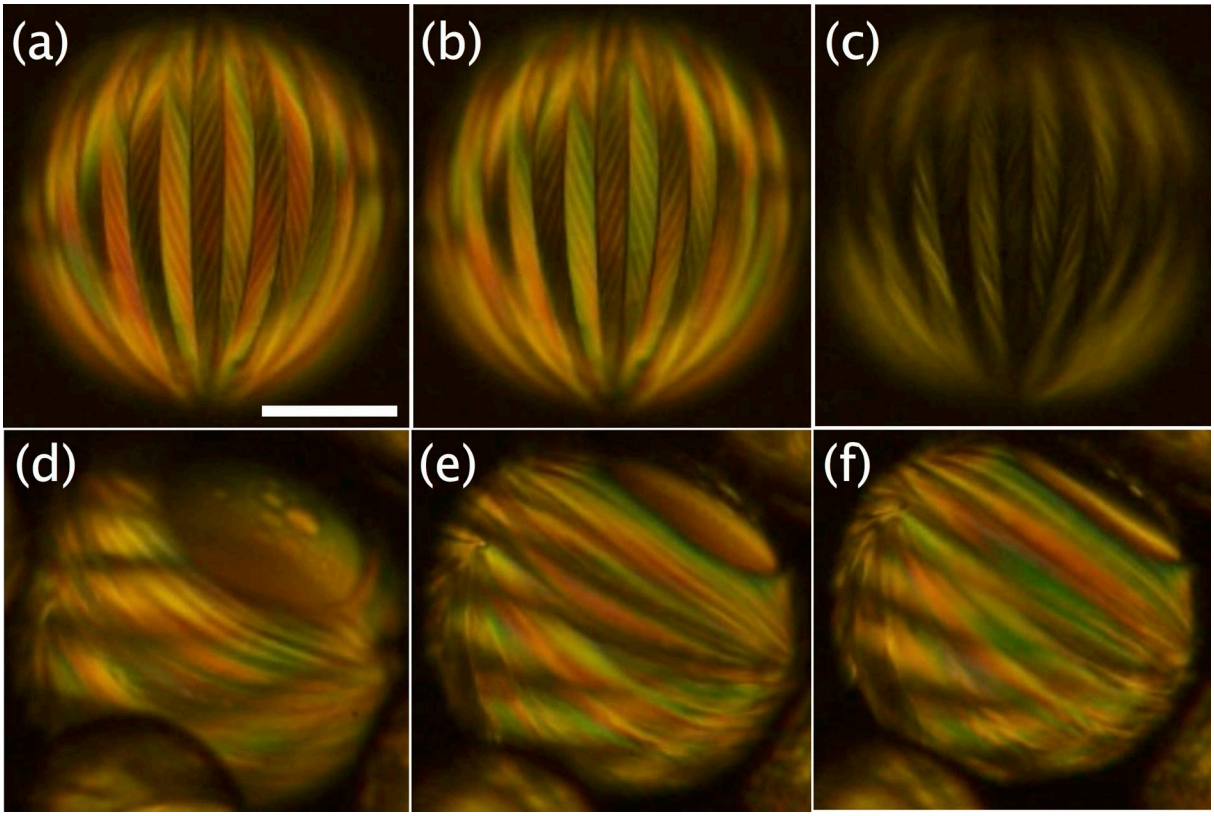

Figure 3. 8CB+RM257 shells polymerized in SmA; (a) immediately after polymerization, (b) after heating to the 8CB nematic phase range, and (c) after heating to the isotropic range of 8CB. (d) A polymerized SmA shell imaged just after flipping the capillary over. (e-f) Gravity rotates the shell back to its original orientation. Scale bar is 50 μm.

Keyword liquid crystals, polymerization, spherical topology, topological defects, microfluidics

JungHyun Noh, Benjamin Henx, Jan P. F. Lagerwall*

Taming liquid crystal self-assembly: the multifaceted response of nematic and smectic shells to polymerization

ToC figure ((Please choose one size: 55 mm broad × 50 mm high **or** 110 mm broad × 20 mm high. Please do not use any other dimensions))

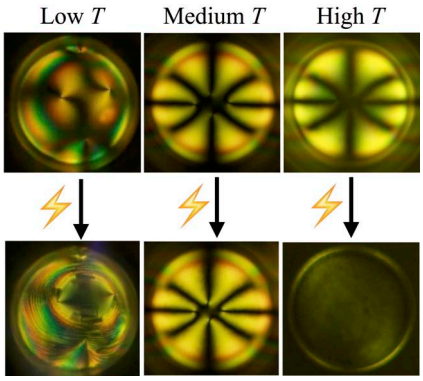

By photopolymerizing liquid crystal shells, their rich variety of self-assembled structures can be rendered permanent and the lifetime extended from days to months, without removing the characteristic responsiveness. If polymerization is carried out close to either boundary of the nematic phase, the process triggers the transition into the adjacent phase, to higher or to lower degree of order.

Submitted to ADVANCED MATERIALS

Supporting Information

for *Adv. Mater.*, DOI: 10.1002/adma.201603158

Taming liquid crystal self-assembly: the multifaceted response of nematic and smectic shells to polymerization

*JungHyun Noh, Benjamin Henx, Jan P. F. Lagerwall**

S1. Experimental details

The photopolymerizable LC mixtures are prepared by adding 5 wt% of an LC-forming diacrylate monomer (4-(3-acryloyloxypropyloxy)benzoic acid 2-methyl-1,4-phenylene ester; RM257, Merck Korea) to a non-reactive LC host (4-cyano-4'-pentyl biphenyl (5CB), 4-cyano-4'-heptyl biphenyl (7CB), 4-cyano-4'-octyl biphenyl (8CB), or 4-cyano-4'-nonyl biphenyl (9CB); Synthon Chemicals, Germany). The lengths of a typical 8CB dimer and of RM257 were estimated using the chemical drawing software Avogadro.

To get a homogeneous mixture, the components are dissolved in excess dichloromethane (Sigma-Aldrich) and the solvent is fully evaporated under stirring at 40°C for one day. Afterwards, the photoinitiator (Irgacure 2022, Ciba) is added, normally at a concentration of 20 wt% with respect to the reactive mesogen component. The reason for this comparatively high concentration of photoinitiator is discussed in Section S9.

LC shells of different mixtures are produced using a coaxial glass capillary microfluidic set-up, adapting the design proposed by Weitz and coworkers.[1] LC and a co-flowing immiscible inner isotropic fluid are flow-focused by a counter-flowing immiscible outer isotropic fluid, enclosing the LC between the two isotropic phases in a double emulsion configuration (Figure S1). The production is performed at elevated temperature, above the clearing point, to lower the viscosity of the LC mixtures, enabling a fine tuning of flow rate to achieve thin shells

below 5 μm in thickness.

In order to ensure planar alignment of the LC, a mixture of water and glycerol (50/50 volume ratio) is used for inner and outer phases, both containing 1 wt% of polyvinyl alcohol (PVA, Mw 13,000 - 23,000 g mol^{-1}, 87-88% hydrolyzed, Sigma-Aldrich) to stabilize the aqueous phase-LC interface. As discussed in an earlier study,[2] the PVA has no aligning effect, adopting a random coil conformation in water solution, but its role is solely to stabilize the shells from coalescence or collapse. The planar alignment is ensured by the contact with the aqueous phase. Due to density mismatch between the inner aqueous phase and the LC, the inner drop sinks to the bottom of the shell in the direction of gravity, rendering the shell asymmetric with thickness decreasing from top to bottom (Figure S2). After shell production, the shells suspended in the outer phase are filled into flat rectangular glass capillaries for optical microscopy. The samples are observed from above in a vertical direction and UV illumination is also carried out from the top.

For high precision temperature control, the capillary containing the shells was placed in a Linkam T95-PE hot stage, used with the cover closed. Under such conditions the temperature gradient over the scale of several shells is negligible, as verified by us previously.[2] In order to have maximum control of the temperature during polymerization, we continuously cooled or heated the sample at a very slow rate, 0.01 K min^{-1}, monitoring the shells continuously with a video camera. Since polymerization takes no longer than one or two minutes, the change in temperature during the process is at most 0.02 K. Notably, the polymerization-induced textural changes occur within seconds from starting the UV irradiation, hence we can safely neglect any effect from the continuous cooling/heating by the hot stage on these phenomena.

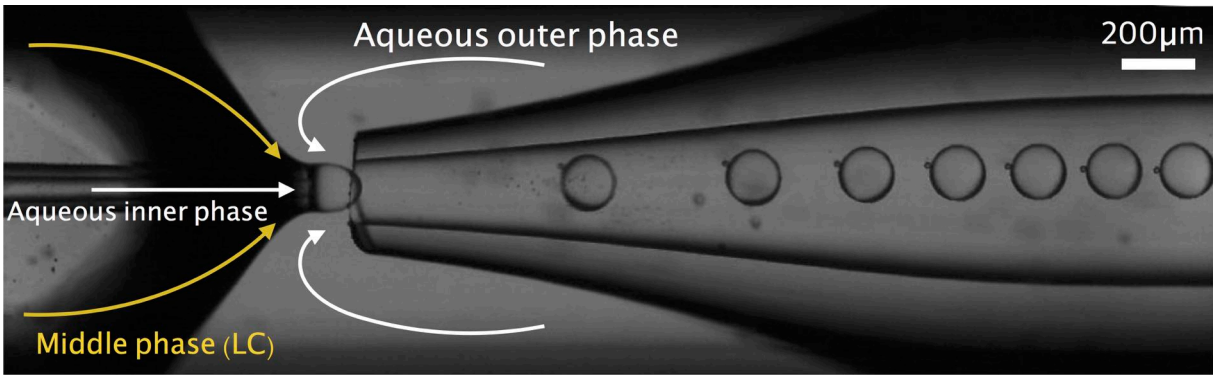

Figure S1: LC shell production using a coaxial glass capillary microfluidic set-up. Small satellite droplets are next to each individual shell. The shells are about 130 μm in diameter and below 3 μm in thickness.

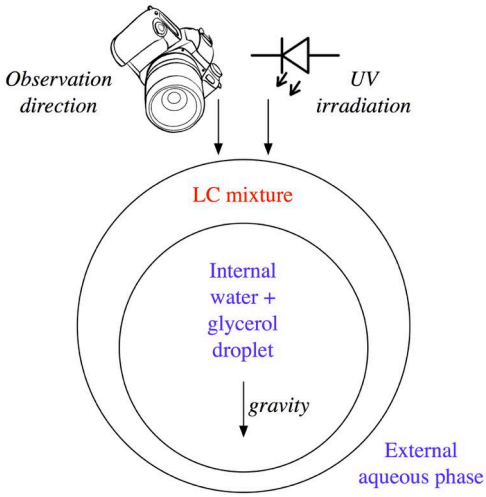

Figure S2: Schematic illustration of the shell cross section, in a plane containing the observation direction and the direction of gravity, illustrating the asymmetry (exaggerated for clarity) of the shell, due to density mismatch between inner fluid and LC mixture.

S2. Transition to the isotropic phase while carrying out polymerization close to the clearing point

When carrying out the photopolymerization of an 8CB+RM257 shell at 41.5°C, slightly below the clearing point, we observe a transition to the isotropic phase during the process.

Figure S3a shows a nematic shell with four tightly-spaced +1/2 defects at 41.5°C before UV exposure. As soon as the shell is illuminated by UV light, the nematic texture 'melts' and gradually disappears (Figure S3b). At the end of the process, it becomes black between crossed polarizers, indicating that it turns isotropic (Figure S3c). As discussed in the main paper, this may be explained by the heat released from the chain reaction of polymerization, under high intensity of UV light, which elevates the temperature locally, taking the system above the clearing point.[3] Afterwards, we cool the sample to 35°C at 10 K min^{-1} and observe countless small-scaled LC domains in the whole shell (Figure S3d), reflecting how the randomly formed polymer network now templates an unnatural mosaic-like configuration of the nematic phase throughout the shell, leading to considerable light scattering (See also SI Movie 2).

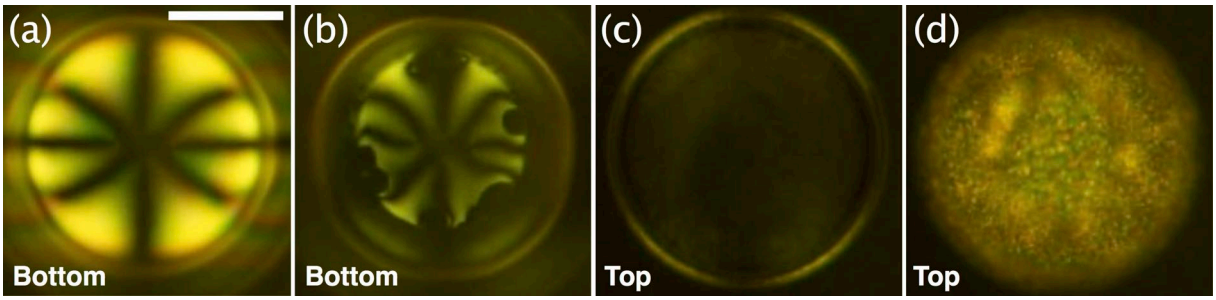

Figure S3: (a-c) Texture changes while the RMs in an 8CB+RM257 shell are polymerized at 41.5°C, close to the clearing point (42.0°C). (a) A pristine nematic shell, displaying four closely-spaced +1/2 defects at 41.5°C. (b) When the shell is exposed to UV light, the nematic texture 'melts' and disappears during polymerization. (c) At the end of the polymerization the shell is black between crossed polarizers. (d) On cooling the polymerized sample to the nematic phase at 35°C after the process, countless domains appear throughout the shell. The focal plane is indicated in each image and the heating and cooling rates are 10 K min^{-1}. Scale bar is 50 μm.

S3. Slow polymerization of 8CB+RM257 nematic shells

In order to investigate the process where polymerization of the RMs induces motion of the defects and induction of a stripe pattern in more detail, we reduce the UV intensity by a factor of ten and double the irradiation time compared to the standard experiments. Figure S4 shows a series of photos while slowly polymerizing an 8CB+RM257 nematic shell at 29.2°C. We confirm that the four defects in the shell gradually move towards the perimeter during polymerization (Figure S4a-c). Specifically, the defect pair labelled 2-3 separates but stays within the focused region of the shell, whereas the defects labelled 1-4 rapidly reach the perimeter, such that they are no longer clearly detectable. This is because the microscope focus remains at the bottom of the shell, below the vertical level of the perimeter, hence these defects are out of focus. At the same time, a new textural development is observed at the bottom part of the shell (Figure S4b-c) with rather irregular stripes. At the end of the process, we could partially observe a chevron pattern with lunes on the left part of the top shell half (Figure S4d), which is not seen in the rapidly polymerized shell (Figure 1d-e in the main paper), but appears in the N-SmA transition in pure 8CB shells.[4, 5]

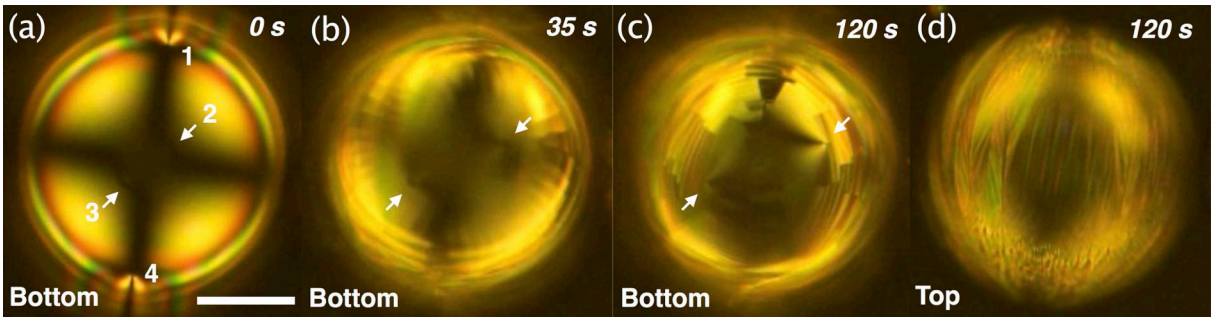

Figure S4: (a-d) Gradual defect movement and textural development in an 8CB+RM257 shell, while the RM is polymerized by a lower intensity of UV light at 29.2°C, which is slightly above the N-SmA transition temperature (29.1°C). The focal plane is indicated in each image. Scale bar is 50 μm.

S4. Proposed explanation for polymerization-induced smectic order

We propose a scenario for the smectic-inducing effect, illustrated schematically in Figure S5. The asymmetric design of nCB-based mesogens leads to antiparallel association into dimers.[6] As illustrated in Figure S5a, the length of such an 8CB dimer (3.56 nm) matches that of the RM257 mesogen (3.6 nm). We assume that the RMs are initially uniformly distributed within the 8CB host, orienting along **n**(**r**) (Figure S5c). On cooling towards T_{NS}, 8CB mesogens organize in a fluctuating smectic-like arrangement, forming cybotactic clusters.[7] When we initiate polymerization, chain propagation takes place perpendicular to **n**, along a plane that effectively defines a smectic layer boundary. This is because the acrylate groups reacting to form the polymer are at each end of the RM257 monomer.

Because of the geometric match between RM257 and the 8CB dimer, we propose that the propagation of the chains renders the cybotactic clusters permanent in time and extends their range in space to the point of divergence, thus breaking the translational symmetry on large scale and inducing the transition to SmA (Figure S5d). In contrast, at high temperatures there are no cybotactic clusters, and the small fraction of RMs is not enough to propagate smectic order over long distances. Instead, polymerization then induces tiny smectic-like islands, probably the scattering grains in Figure 1b in the main paper.

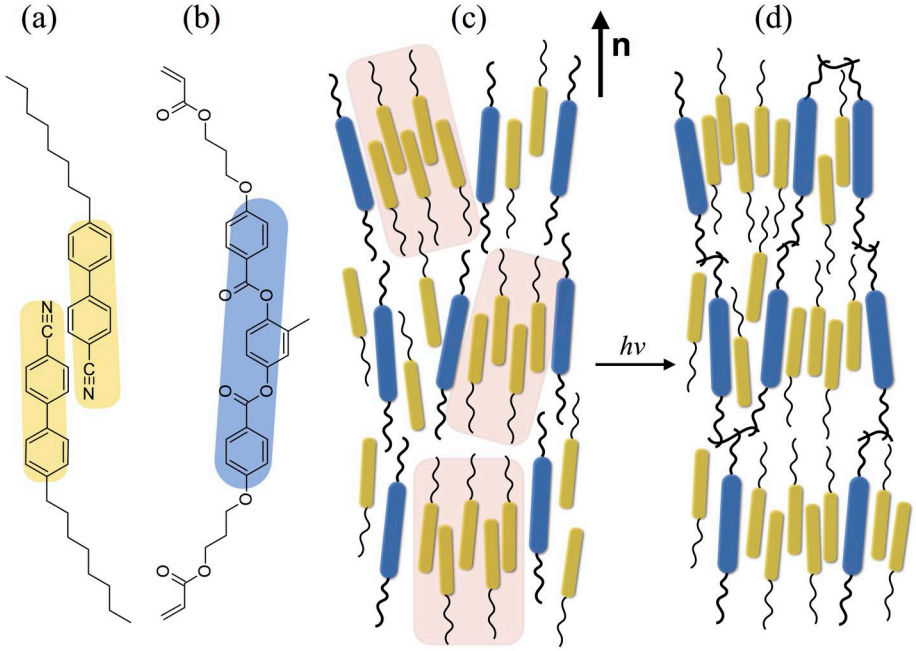

Figure S5: (a-b) Chemical structures of dimerized 8CB and RM257, with highlighted core regions. (c-d) Schematic drawing of a potential scenario during photopolymerization; (c) 8CB forms pre-smectic clusters (red) upon approaching the N-SmA transition. (d) Upon photopolymerization the cluster size diverges.

S5. Polymerization of 7CB+RM257 nematic shells

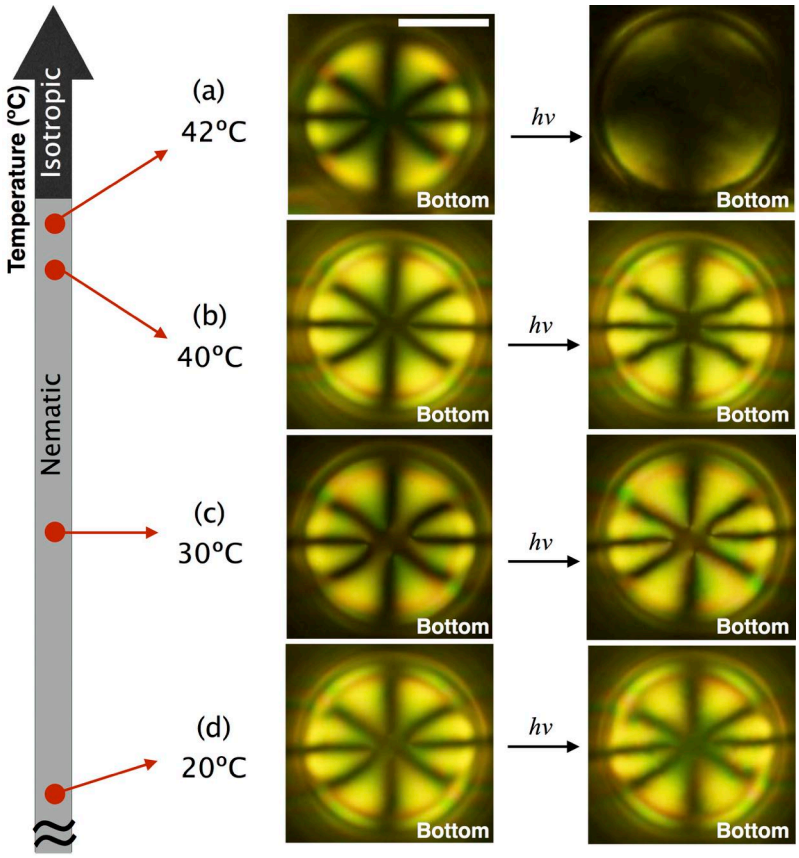

Figure S6: Polarizing microscopy textures of pristine 7CB+RM257 nematic shells (left) and polymer-stabilized shells (right), the polymerization taking place at four selected temperatures; (a) 42°C, (b) 40°C, (c) 30°C indicated in each image. Scale bar is 50 μm.

An interesting question is whether a smectic phase could be induced by polymerization even if the shell is made of an LC mixture that does not exhibit a SmA phase in its equilibrium phase diagram. To explore this question we prepare shells from a photopolymerizable mixture where we have replaced 8CB with 7CB, which exhibits a nematic phase but no SmA phase. The mixture contains the same quantity of RM257 and photoinitiator as used with the 8CB shells, discussed in detail in the main paper. We perform rapid polymerization of different shells, at varying nematic temperatures (Figure S6). While the polymerization-induced loss of

LC order at high temperature could be reproduced also with these shells (Figure S6a), indicative of a reaction-induced temperature increase, there was no sign of inducing smectic order, regardless of temperature. As seen in Figure S6b-d, we tested by polymerizing at 40°C, 30°C and 20°C, respectively, never observing any smectic induction. Note that crystallization takes place at lower temperature in the mixture than in pure 7CB (30°C) and that some supercooling of the nematic state in this shell is common. This confirms that we need the vicinity to an N-SmA phase transition and the presence of cybotactic clusters to induce the transition by polymerization, at least when the RM concentration is low.

S6. Polymerization of a 5CB+RM257 nematic shell

We explored also mixtures based on the common nematogen 5CB, finding the same results (Figure S7). There was no smectic-inducing effect on polymerizing 5CB+RM257 nematic shells. As discussed in the previous section on 7CB-based shells, this is due to the lack of cybotactic clusters, since 5CB does not show smectic behavior in a phase sequence. Instead, we see a somewhat grainy texture (Figure S7b), with increased light scattering, in the 5CB-based shell after the RM257 component had been polymerized at 30°C.

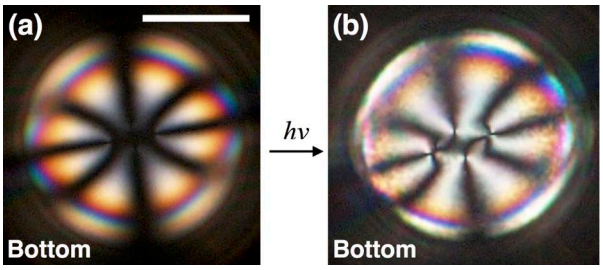

Figure S7: Polarizing microscopy textures of (a) a pristine 5CB+RM257 nematic shell and (b) the shell after polymerization of the RM at 30°C, at which the LC is in the nematic phase. The focal plane is indicated in each image. Scale bar is 50 μm.

S7. Polymerization of 9CB+RM257 nematic shells

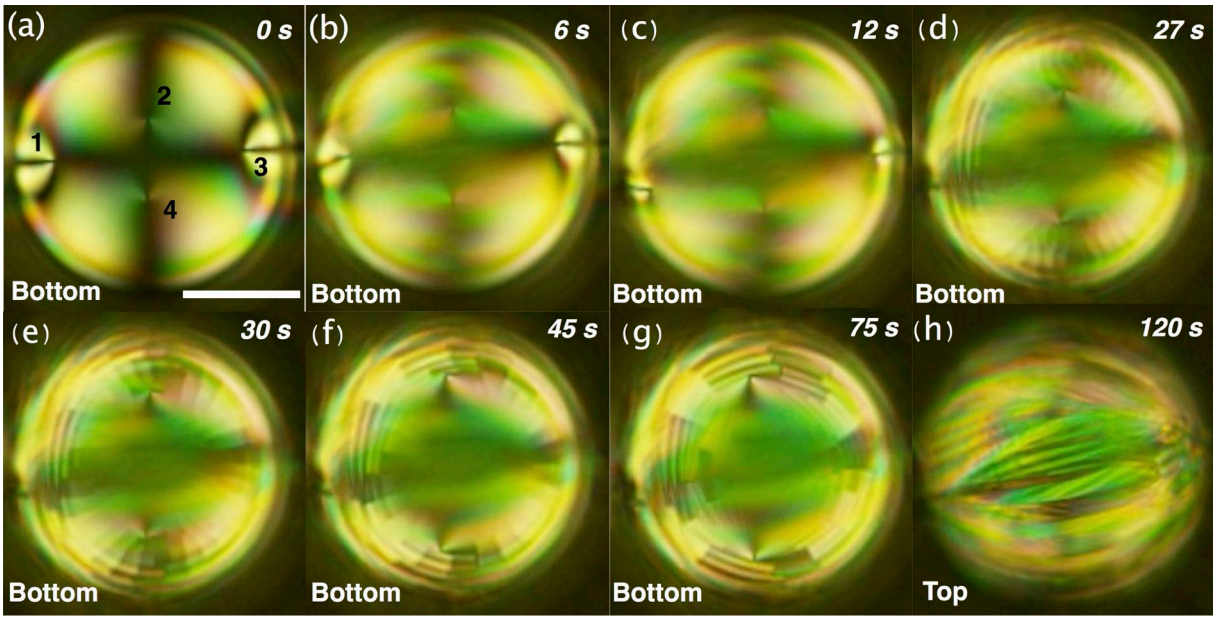

Figure S8: (a-h) Gradual defect movements and textural development in an 9CB+RM257 shell, while the RM component is polymerized by a lower intensity of UV light, at 44°C, slightly above the SmA-N transition temperature (43.3°C). Overall, the shell looks yellow-greenish because of inserting a yellow filter during the observation. Time indicates the time after the shell was exposed to UV light. The focal plane is indicated in each image. Scale bar is 50 μm.

In order to rule out that the difference in behavior between shells based on 7CB and 8CB, respectively, is an odd-even e↵ect with respect to the length of the alkyl chain,[6] we finally studied shells of 9CB+RM257 (Figure S8). In contrast to 7CB, 9CB exhibits an N-SmA phase transition, like 8CB, although it has an odd number of carbons in the alkyl chain. In the presence of RM257 in pure 9CB, the SmA-N transition temperature is shifted from 47.5°C to 43.3°C. On cooling a pristine 9CB+RM257 nematic shell towards T_{SN} (43.3°C), we observe the same behavior as in 8CB-based shells, with four defects starting to approach the perimeter

at 44°C (Figure S8a). Illuminating with low intensity UV light to induce polymerization of the RM component, we again clearly see a gradual defect migration to the perimeter (Figure S8b-c). Likewise, stripes appear at the bottom part of the shell (Figure S8d-g), together with a lune pattern that is most clearly seen at the top half of the shell (Figure S8h), analogous to the SmA texture in pure 8CB shells.[4, 5] We thus conclude that the requirement for inducing smectic order by polymerization is that already the host exhibits this phase inherently, whereas no odd-even effect seems to exist in this respect.

S8. Cooling a polymerized 7CB+RM257 shell to 0°C

To test the temperature stability of polymer-stabilized shells at low temperature, we cool 7CB+RM257 nematic shells down to 0°C, which is far below the normal LC temperature range, after polymerization at 30°C (Figure S9). Since the aqueous inner and outer phases contain glycerol and PVA, they can remain fluid without ice formation at 0°C.

Figure S9a shows three polymerized shells at 30°C, with a higher order birefringence color com- pared to the previous shells in Figure S6. This is because the polymerized shells are slightly rotated from the initial position, where the defects were located at the thinnest, bottom part of the shell, as defined by the vertical direction of the microscope. In the initial situation, birefringence of top and bottom surfaces can partially cancel out when the director fields are perpendicular to each other. However, when the shells rotate, the director fields are not perpendicular anymore in a vertical light path, increasing the effective birefringence in our viewing direction.

On cooling the polymerized shells to 0°C at 10 K min^{-1}, the shells still keep their shape without rupture and no textural change is seen (Figure S9b). This confirms their outstanding stability against dramatic temperature changes. The photo in Figure S9b looks cloudy

compared to the photo in (a), taken at 30°C. This is due to condensation of water droplets on the outer surface of the glass capillary when cooling down towards 0°C.

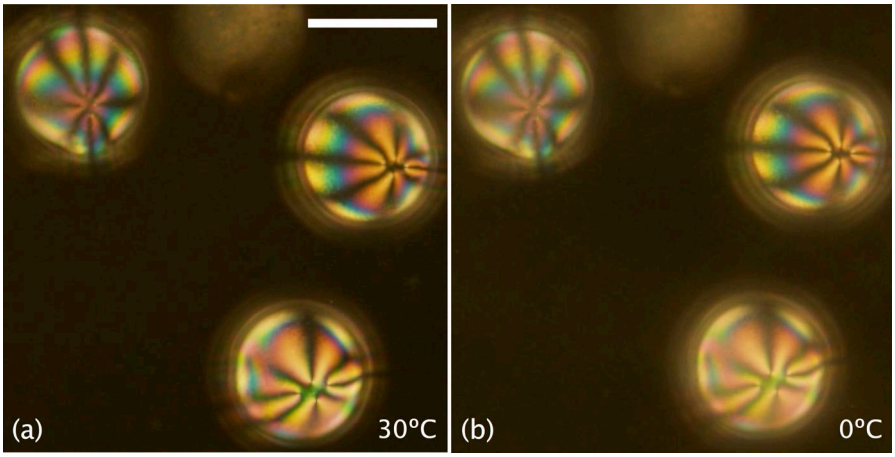

Figure S9: Cooling the polymer-stabilized 7CB+RM257 shells (a) from 30°C (b) to 0°C. The RMs are polymerized at 30°C and the scale bar is 100 μm.

S9 Impact of the amount of photoinitiator added to the LC+RM precursor mixture

In most experiments the concentration of photoinitiator was 20 wt% with respect to RM257, which is a rather high concentration compared to previous LC photopolymerization studies. More common is to use about 1% photoinitiator with respect to the monomer concentration. The reason for our unusually large concentration of photoinitiator is that the mixture in which polymerization takes place is surrounded by aqueous phases on both sides. Since the shells are thin, in particular at the bottom, this means that there is a considerable risk of oxygen dissolved in the aqueous phases diffusing into the reactive mixture. As oxygen is a strong polymerization inhibitor, our strategy to counteract its influence was to drastically increase the amount of photoinitiator, allowing the excess initiator to act as an oxygen scavenger and thereby minimize the undesired premature termination of the polymerization reaction.

To corroborate our assumption, we carried out a number of reference experiments with

varying concentrations of photoinitiator in the different phases of our system. Figure S10 shows the effect of polymerization at 35°C in nematic 8CB+RM257 shells containing photoinitiator at concentrations (with respect to the concentration of RM257) 1 wt% and 10 wt%, respectively. The bottom surfaces, at which the topological defects are collected due to the geometric shell asymmetry, retain the nematic texture after polymerization. The top surfaces of the two shells become somewhat grainy after polymerization, which is the same result as with the 20 wt% photoinitiator shell shown in Figure 1b in the main paper.

After polymerization, we heat the shells above the clearing point (Figure S11). As in the shell polymer-stabilized with 20 wt% photoinitiator, we observe a loss of birefringent texture on the bottom, defect-rich half of both shells (Figure S11b/g), whereas the top half in both cases reveals high remaining birefringence after rotating the crossed polarizers with respect to the sample (Figure S11c/h). The birefringence is stronger with 10% photoinitiator than with 1%, suggesting that the polymer network is denser with a higher photoinitiator concentration.

When cooling the shells to 35°C to regain the nematic phase, the shell bottoms initially develop schlieren textures that are more irregular than usual (Figure S11d/i), even with more than four defects for a considerable amount of time. After several minutes the normal equilibrium texture with four defects at the shell bottom is again established (Figure S11e/j), but the process is different from unpolymerized shells as well as from shells polymerized with higher concentration of photoinitiator. Moreover, in contrast to the latter case, the stable defect arrangement is not quite identical to that prior to heating.

With the lower concentration of photoinitiator, we believe that the inhibiting action of oxygen strongly influences the process. At any interface to an aqueous phase the polymer chain growth is rapidly terminated by the high availability of oxygen and a large-scale polymer network cannot form. The effect is the most detrimental at the bottom of the shell, which is

the thinnest point, thus the most exposed to oxygen. At the shell top the liquid crystal layer may be thick enough that polymerization can continue over large scale near the middle of the liquid crystal, to which the diffusion of oxygen is not fast enough to inhibit the reaction.

This means that a continuous polymer network, templated by a uniform nematic director field, grows along the shell top, explaining the remaining birefringence after polymerization. At the shell bottom, in contrast, only oligomers or small isolated patches of polymer are able to form before the reaction is inhibited, leading to the loss of birefringence upon heating. When the shell is heated to the isotropic phase, the disconnected polymerized patches rearrange at random, as the long-range order of the host is gone. Thus, rather than stabilizing the original director field when the shell is cooled back to the nematic phase, they will template ordering in random directions at different points. They thereby induce many more defects than usual, until after several minutes the patches have been reorganized into an arrangement that is compatible with the usual four-defect director field. This explains the unusually defect-rich transient texture in Figure S11d/i.

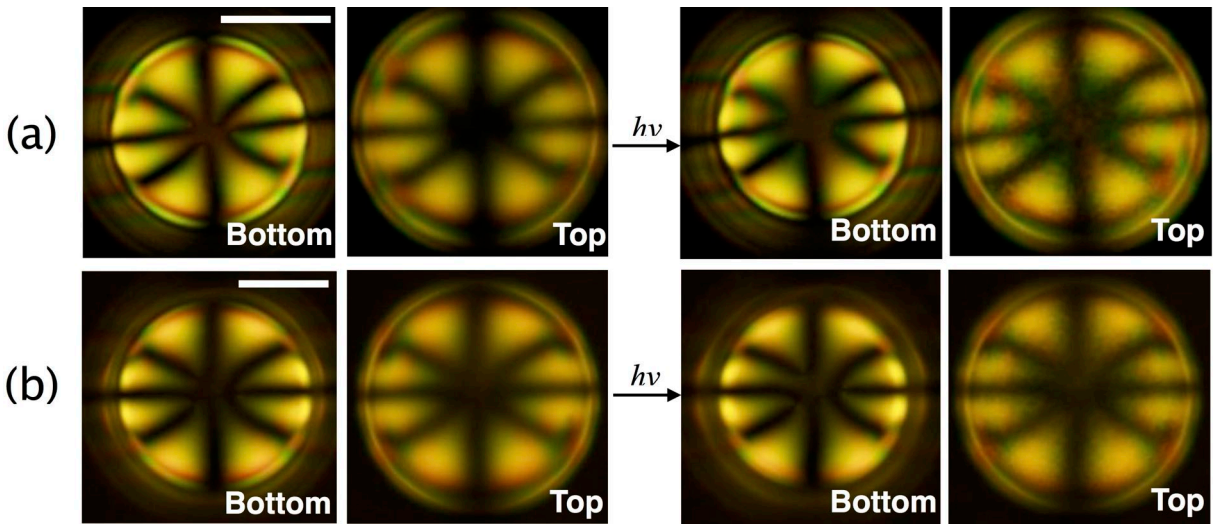

Figure S10: Polarizing microscopy textures of pristine 8CB+RM257 nematic shells with di↵erent concentrations of photoinitiator (left), and the corresponding shells after polymerization at 35 C of the RM (right). The concentration of photoinitiator, with respect to

RM, is (a) 1 wt% and (b) 10 wt%, respectively. Scale bar is 50 μm.

By flipping over capillaries filled with the polymer-stabilized shells, the shells rotate by gravity, as discussed in the main paper in connection to Figure 3. During the rotation, we observe the shells without analyzer and between crossed polarizers, consecutively. For both shell types we see the grainy texture of a large-scale polymerized top half, while the bottom half shows a smooth texture, as expected if only a minor amount of polymer is present here. In addition, we observe a rather sharp boundary, highlighted by white dashed lines and arrows in Figure S12, that separates the continuously polymerized top shell half from the largely unpolymerized bottom half.

By increasing the photoinitiator concentration to 20% the inhibiting action of oxygen can be partially counteracted by the excess photoinitiator, effectively acting as an oxygen scavenger during polymerization. This allows the polymer network to grow throughout the shell, extending even through the thinnest part. However, even in this case the network growth suffers frequent interruptions due to oxygen, explaining why the final polymer network is so sparse on the thinner side that the phase transition from nematic to isotropic can take place on this shell half, although the continuity of the network ensures that the defect configuration is fixed.

As a final confirmation of the importance of oxygen as inhibitor we also prepared shells with 1wt% photoinitiator in the LC mixture but now we added 0.1wt% of water-soluble photoinitiator (2-hydroxy-4’-(2-hydroxyethoxy)-2-methylpropiophenone) to both surrounding phases, inside and outside the shells. This means that the oxygen scavenger is present outside the LC, allowing us to work with a more typical photoinitiator concentration in the reactive LC mixture. Indeed, when these shells were irradiated by UV light we could confirm (Figure

S13) polymer network formation throughout the shell, with a result very similar to the case when 20wt% photoinitiator was added to the LC, without initiator in the aqueous phases.

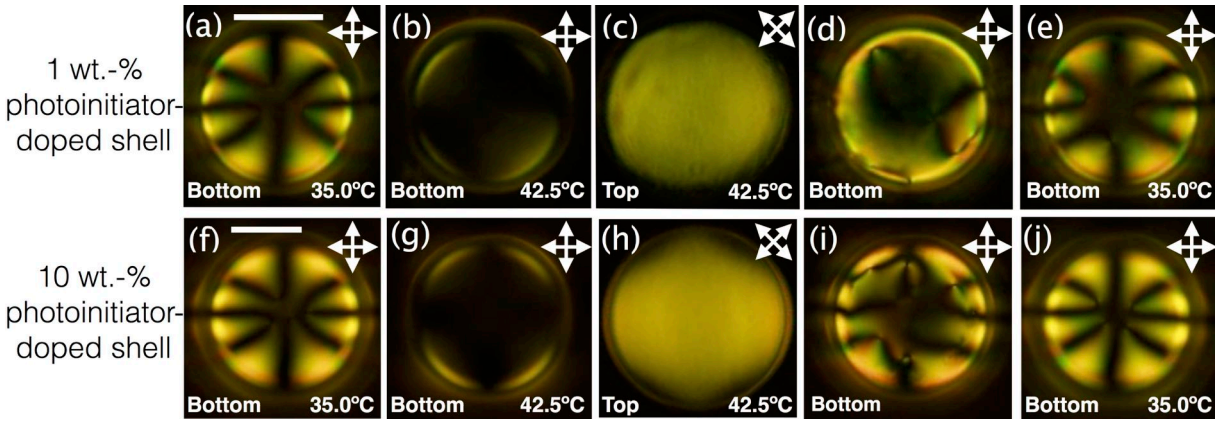

Figure S11: Texture changes on heating and cooling (a-e) 1 wt% and (f-j) 10 wt% photoinitiator-containing 8CB+RM257 shells, respectively, after polymerization of the RM at 35°C in nematic phase. (a, f) Polymerized nematic texture with four +1/2 defects at the bottom part of the shell at 35°C. (b, g) Texture at 42.5°C, above the clearing point at 42.0°C. (c, h) A highly birefringent polymer network is observed at the top half of each shell when rotating the crossed polarizers by 45° to the samples. (d, i) On cooling towards 35°C at nematic phase, random schlieren textures appear at the bottom half of the shells, and somewhat afterwards (e, j) defects with total charge of +2 are recovered at the bottom surfaces. The configuration is similar but not quite identical to that prior to heating. The focal plane is indicated in each image. The heating and cooling rates are 10 K min^{-1}. Scale bar is 50 μm.

S10. Impact of the UV illumination direction

It has been well established that photopolymerization is more efficient on the side close to the

UV light source,[8, 9, 10] due to the light absorption by the photoinitiator at the illuminated side reducing the UV intensity further into the sample. This leads to faster polymerization on the irradiated side, depleting the monomers more rapidly on this side, thus inducing diffusion of monomers from the unilluminated to the illuminated side, thereby creating a gradient in polymer density. To some extent this mechanism must be active also in our shells, but the following experiment indicates that it appears to be secondary to the influence of the oxygen inhibitor diffusing from the surrounding aqueous phases.

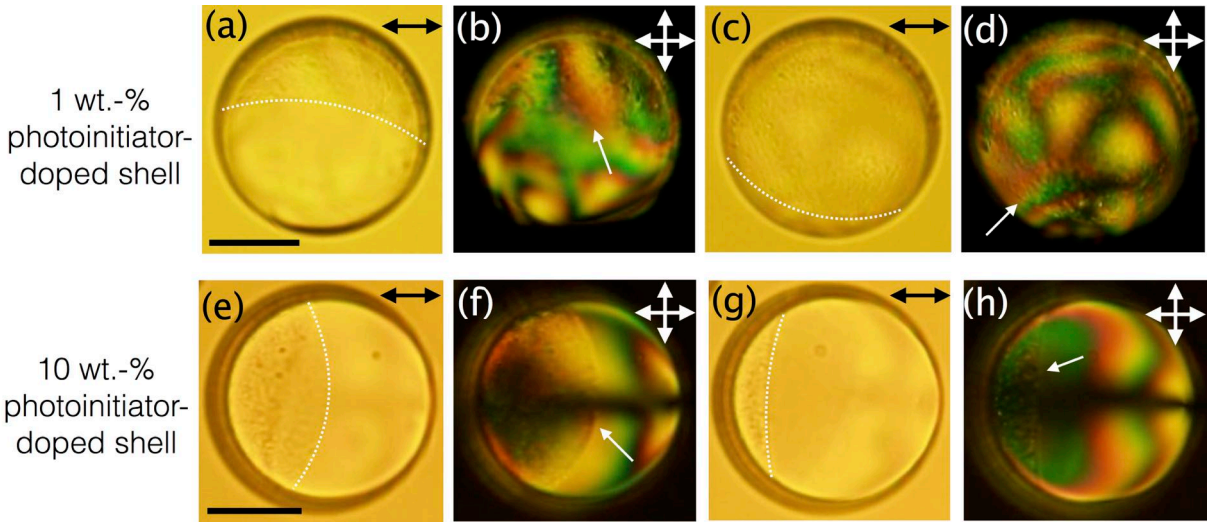

Figure S12: Sideviews of shells after polymerization with (a-d) 1 wt% and (e-h) 10 wt% photoinitiator, respectively, while the shells are rotated by gravity. Each row is one sequence, time passing from left to right. We observe the rotating shells without analyzer (a/e and later c/g) and between crossed polarizers (b/f and later d/h), consecutively. The white dashed lines and arrows indicate the boundary between continuously polymerized top shell half and largely unpolymerized bottom shell half. Scale bar is 50 µm.

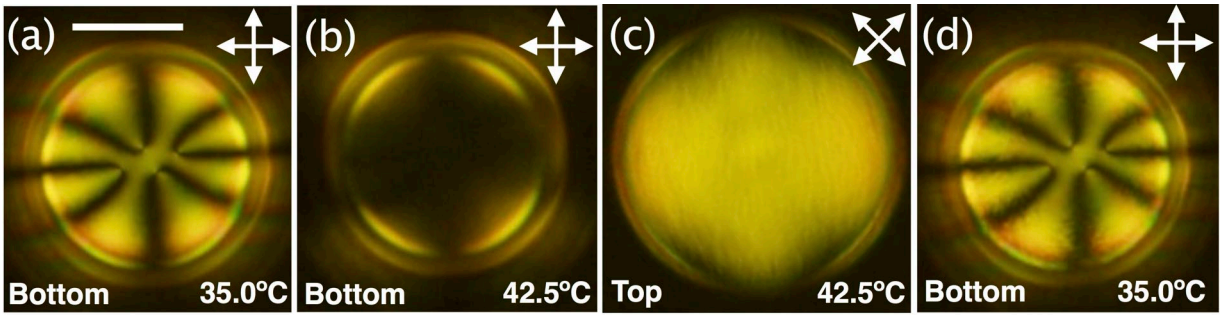

Figure S13: Textural response to heating and cooling of a shell containing 1% photoinitiator, surrounded by aqueous phases to which water soluble photoinitiator was added, after UV-initiated polymerization of the RM component. The polymer network now extends throughout the shell, albeit with greater thickness at the top than at the bottom.

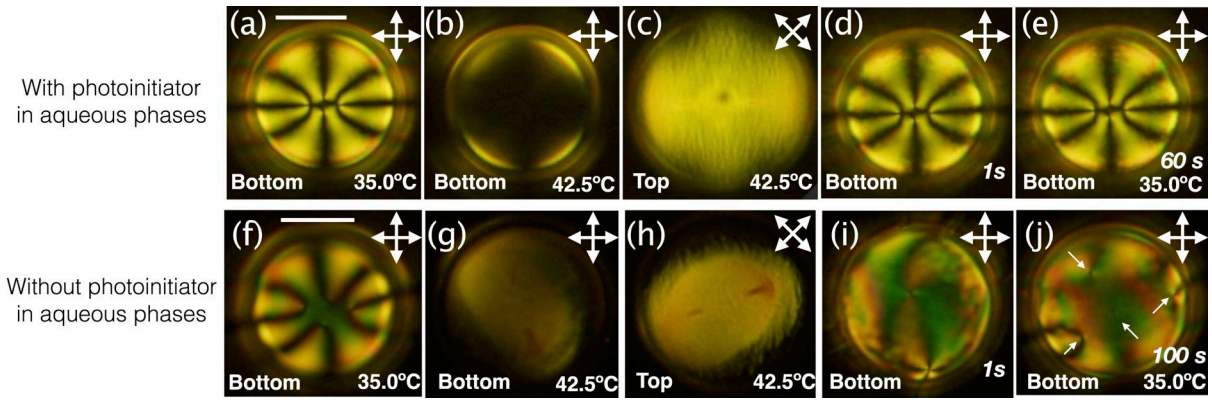

Figure S14: Textural response to heating and cooling of a shell containing 1% photoinitiator, surrounded by aqueous phases containing photoinitiator (top row) and without photoinitiator (bottom row), after polymerization of the RM component by UV irradiation from below. The behavior is identical to corresponding shells polymerized by UV irradiation from above.

We prepared a set of shells with 1wt% photoinitiator in the LC mixture, in one case with aqueous phases containing water soluble photoinitiator, in another case with the regular aqueous phases, and irradiated these shells with UV light from the bottom rather than from the top, see Figure S14. In both cases we had essentially identical results to when the irradiation was from the top: the thick side of the shell developed a connected, dense and aligned polymer network that remained birefringent after the shell was heated above the clearing point of the host, whereas the thin side became black with a loss of the schlieren texture and the defects at high temperature. Upon cooling back into the nematic phase, the results were again the same as for the corresponding shells irradiated from above: when photoinitiator had been added to the aqueous phases the bottom immediately regained the original director field, whereas the shells prepared without photoinitiator in the surrounding phases first developed a defect-rich disordered schlieren texture, which only slowly relaxed to the ordinary texture with four defects at the shell bottom.

S11. Absorbance of individual components of the 8CB+RM257 shell

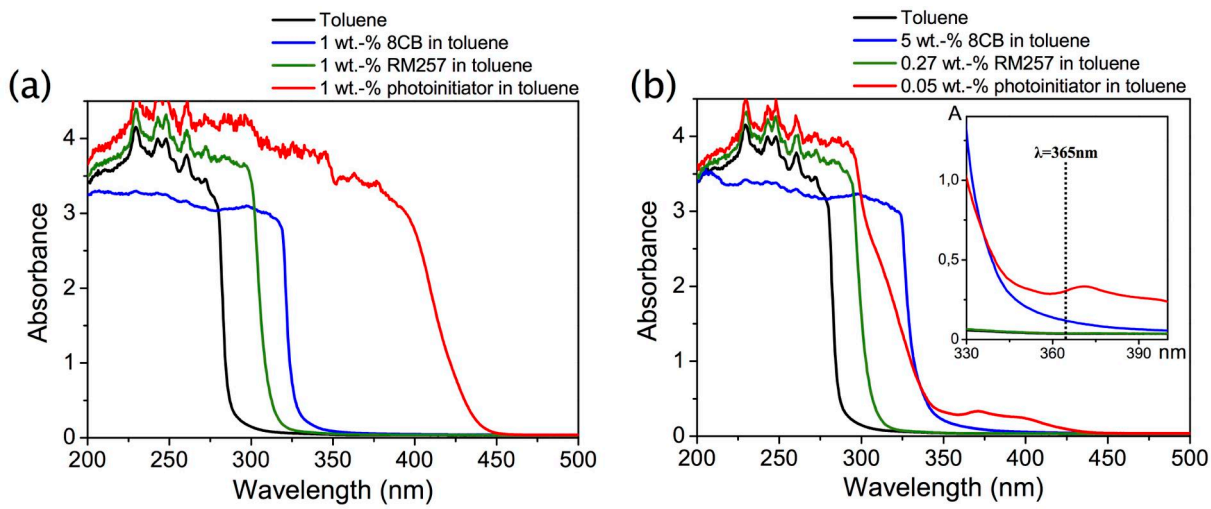

Figure S15: Absorbance of the liquid crystal shell components; (a) Each solute is measured at 1 wt% in toluene. (b) The three solutes are measured at the same relative concentrations as in the shell, 8CB : RM257 : photoinitiator = 94 : 5 : 1.

[1] A. Utada, L. Chu, A. Fernandez-Nieves, D. Link, C. Holtze, and D. Weitz, *MRS Bull.*, **2007**, *32*, 702.

[2] J. Noh, K. Reguengo De Sousa, and J. P. F. Lagerwall, *Soft Matter*, **2016**, *12*, 367.

[3] D. J. Broer, N. Grietje, and N. Mol, *Makromol. Chem.*, **1991**, *192*, 59.

[4] T. Lopez-Leon, A. Fernandez-Nieves, M. Nobili, and C. Blanc, *Phys. Rev. Lett.*, **2011**, *106*, 247802.

[5] H.-L. Liang, S. Schymura, P. Rudquist, and J. Lagerwall, *Phys. Rev. Lett.*, **2011**, *106*, 247801.

[6] D. Demus, J. W. Goodby, G. Gray, H.-W. Spiess, V. Vill, *Handbook of liquid crystals.*, Wiley-VCH, Weinheim, **1998**.

[7] A. De Vries, *Mol. Cryst. Liq. Cryst.*, **1970**, *10*, 219.

[8] D. J. Broer, J. Lub, and N. Mol, *Nature*, **1995**, *378*, 467.

[9] C. L. van Oosten, D. Corbett, D. Davies, M. Warner, C. W. M. Bastiaansen, and D. J. Broer, *Macromolecules*, **2008**, *41*, 8592.

[10] S. Relaix, C. Bourgerette, and M. Mitov, *Liq. Cryst.*, **2007**, *34*, 1009.